

Experimental realization of a Dirac monopole through the decay of an isolated monopole

T. Ollikainen,^{1,2,*} K. Tiurev,¹ A. Blinova,² W. Lee,^{2,†} D. S. Hall,² and M. Möttönen^{1,3}

¹*QCD Labs, COMP Centre of Excellence, Department of Applied Physics, Aalto University, P.O. Box 13500, FI-00076 Aalto, Finland*

²*Department of Physics and Astronomy, Amherst College, Amherst, MA 01002-5000, USA*

³*University of Jyväskylä, Department of Mathematical Information Technology, P.O. Box 35, FI-40014 University of Jyväskylä, Finland*

We experimentally observe the decay dynamics of deterministically created isolated monopoles in spin-1 Bose–Einstein condensates. As the condensate undergoes a transition between magnetic phases, the isolated monopole gradually transforms into a spin configuration hosting a Dirac monopole in its synthetic magnetic field. We characterize in detail such a Dirac monopole by measuring the particle densities of the spin states projected along different quantization axes. Importantly, we observe the spontaneous emergence of nodal lines in the condensate density that accompany the Dirac monopole. We also demonstrate that the monopole decay accelerates in weaker magnetic field gradients.

I. INTRODUCTION

Spinor Bose–Einstein condensates (BECs) of alkali atom gases [1, 2] offer an exceptionally versatile platform to study various topological defects [3]. These defects are qualitatively nontrivial configurations in the order parameter fields of BECs and, by definition, they are robust against perturbations.

In addition to displaying the scalar properties of a superfluid, spinor BECs exhibit intriguing magnetic order in their spin degrees of freedom. Consequently, the spectrum of topological defects available in spinor systems is rich, including vortices [4–7], coreless vortices [8, 9], half-quantum vortices [10], solitonic vortices [11], skyrmions [12–14], monopoles [15–20], and knots [21, 22]. Although the defects are topologically stable and remain essentially intact for the duration of the creation process [15–22], there may be decay channels rendering them dynamically unstable [23].

The natural magnetic phase of an atomic spin-1 BEC is either ferromagnetic or polar [24], depending on the atomic species. With higher-dimensional internal structure, even more magnetic phases are available [25]. Interestingly, the spin degree of freedom can give rise to synthetic electromagnetism, in which a part of the BEC order parameter acts as a charged quantum particle in the presence of synthetic electromagnetic potentials arising from spatiotemporal variations of its spinor [26–28].

We are especially interested in gauge potentials that give rise to a monopole in the synthetic magnetic field. Creation of such a Dirac monopole in a ferromagnetic BEC was recently proposed [18] and implemented experimentally [19], providing the first known realization of Dirac’s celebrated theory of a charged quantum parti-

cle interacting with a fixed magnetic monopole [29]. We stress that such a Dirac monopole is not accompanied by a topological point defect in the ferromagnetic order parameter as the location of the monopole is connected to the condensate boundary by a so-called nodal line, along

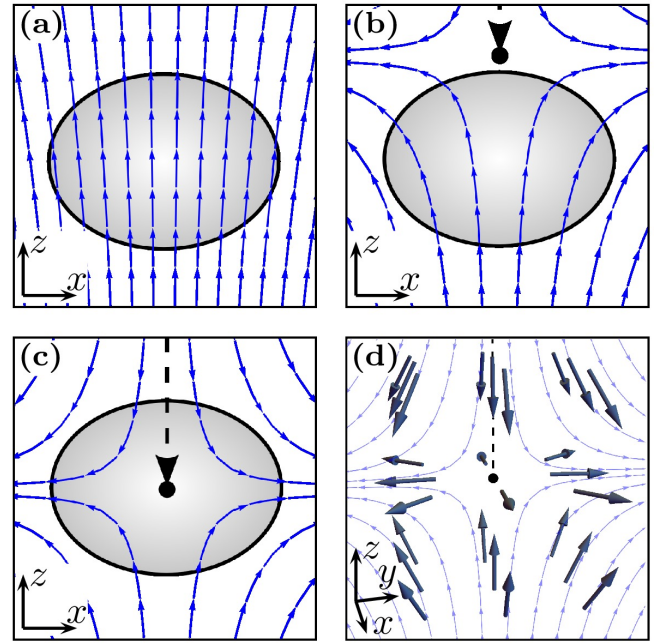


FIG. 1. Creation process of the isolated monopole. (a–c) The control sequence of the external quadrupole magnetic field (blue thin arrows) during the creation process and (d) the theoretical spin configuration generating a Dirac monopole. The zero point of the quadrupole magnetic field, indicated by the black dot, is (a) well above, (b) approaching, and (c) in the middle of the condensate (shaded ellipse). The dashed arrow in (b–d) shows the path traced by the zero point as it is brought into the condensate. In (d), the centers of the arrows indicate the direction of local spin at selected points in space.

* tuomas.ollikainen@aalto.fi

† Present address: Department of Physics, Princeton University, Princeton, NJ 08544, USA

which the condensate density vanishes.

Another recent experiment [20] reported the first observation of isolated monopoles, i.e., topological point defects, in the polar phase of a spin-1 ^{87}Rb BEC. The creation process is illustrated in Fig. 1(a–c). Although the point defect is created in the polar phase, the magnetic phase for the ground state of a ^{87}Rb BEC is ferromagnetic. It is therefore natural that the condensate eventually decays from the polar phase into the ferromagnetic phase. Interestingly, recent theoretical results [30] show that a polar BEC with an isolated monopole will evolve into a ferromagnetic spin configuration with a Dirac monopole in its associated synthetic magnetic field. However, experimental studies of this intriguing phenomenon are lacking to date.

We report here the experimental observation of the decay dynamics of an isolated monopole in a ^{87}Rb spin-1 BEC. In good agreement with theoretical predictions [30], the condensate experiences a dynamical quantum phase transition from the polar to the ferromagnetic phase. This transition gives rise to the decay of the isolated monopole defect in the order parameter into a Dirac monopole in the accompanying synthetic magnetic field. We draw evidence for our conclusions from observations of the column particle densities in different spin states during the decay. The Dirac monopoles are connected to the condensate boundary by nodal lines of vanishing particle density in the ferromagnetic phase. In previous experiments [19], these nodal lines were deterministically created as doubly-quantized vortices terminating at the monopole. In contrast, the nodal lines here appear spontaneously as a pair of connected, singly-quantized vortex lines.

We further characterize the Dirac monopole by projecting the condensate spin texture along three perpendicular quantization axes. These projections provide additional evidence that the ground-state spin configuration contains a Dirac monopole in its synthetic magnetic field. We compare our experimental results to numerical simulations, and find them to be in good agreement. We study the decay rate utilizing the time-dependent magnetization of the condensate.

This paper is organized as follows: In Sec. II, we provide the necessary theoretical background for describing the monopole defects and their creation protocol in spin-1 BECs. In Sec. III, we present the employed experimental and numerical methods. Section IV is devoted to the experimental results on the decay dynamics and comparison with corresponding numerical simulations. We provide reflections on our results in Sec. V.

II. THEORY

We base our analysis on the zero-temperature mean-field order parameter of the spin-1 BEC

$$\Psi(\mathbf{r}, t) = \sqrt{n(\mathbf{r}, t)} e^{i\phi(\mathbf{r}, t)} \zeta(\mathbf{r}, t), \quad (1)$$

where n is the particle density, ϕ is the scalar phase, and $\zeta = (\zeta_{+1}, \zeta_0, \zeta_{-1})^T$ is a three-component complex-valued spinor satisfying the normalization condition $\zeta^\dagger \zeta = 1$. Here, ζ is expressed in the basis of the z -quantized spin states $\{|1\rangle, |0\rangle, |-1\rangle\}$. In general, the spinors for the ferromagnetic and polar phases in this basis read [24]

$$\zeta_F = \mathcal{U}(\alpha, \beta, \gamma) \begin{pmatrix} 1 \\ 0 \\ 0 \end{pmatrix}_Z = e^{-i\gamma} \begin{pmatrix} e^{-i\alpha} \cos^2 \frac{\beta}{2} \\ \sqrt{2} \cos \frac{\beta}{2} \sin \frac{\beta}{2} \\ e^{i\alpha} \sin^2 \frac{\beta}{2} \end{pmatrix}_Z, \quad (2)$$

and,

$$\zeta_P = \mathcal{U}(\alpha, \beta, \gamma) \begin{pmatrix} 0 \\ 1 \\ 0 \end{pmatrix}_Z = \frac{1}{\sqrt{2}} \begin{pmatrix} -e^{-i\alpha} \sin \beta \\ \sqrt{2} \cos \beta \\ e^{i\alpha} \sin \beta \end{pmatrix}_Z, \quad (3)$$

where $\mathcal{U} = e^{-iF_z\alpha} e^{-iF_y\beta} e^{-iF_z\gamma}$ is the general spin rotation operator with Euler angles α , β , and γ , and F_y and F_z are the standard dimensionless spin-1 matrices. The subscripts F and P are used to refer to the ferromagnetic and polar phase, respectively.

The spinor in the polar phase can alternatively be written as

$$\zeta_P = \frac{1}{\sqrt{2}} \begin{pmatrix} -d_x + id_y \\ \sqrt{2} d_z \\ d_x + id_y \end{pmatrix}_Z, \quad (4)$$

where $\hat{\mathbf{d}} = (d_x, d_y, d_z)^T = (\cos \alpha \sin \beta, \sin \alpha \sin \beta, \cos \beta)^T$ is a real-valued unit vector defining the direction of nematic order in the condensate, i.e., the spinor is in the eigenstate of $\mathbf{F} \cdot \hat{\mathbf{d}}$ with the eigenvalue $m_F = 0$. Here, $\mathbf{F} = (F_x, F_y, F_z)^T$ is a vector of the dimensionless spin-1 matrices. The polar order parameter may thus be expressed as $\Psi = \sqrt{n} e^{i\phi} \hat{\mathbf{d}}$ in the Cartesian basis. We use the vector field described by $\hat{\mathbf{d}}$ to characterize topological defects in the polar phase.

In the ferromagnetic phase, the length of the local spin is unity, whereas in the pure polar phase it vanishes. Hence, in the ferromagnetic phase, the local average spin

$$\mathbf{S}(\mathbf{r}) = \zeta(\mathbf{r})^\dagger \mathbf{F} \zeta(\mathbf{r}), \quad (5)$$

can be conveniently used in the characterization of possible topological defects.

The order parameter space in the polar phase is given by $\mathcal{O}_P \cong [\text{U}(1) \times S^2] / \mathbb{Z}_2$ [31], allowing the existence of singular point defects due to the nontriviality of the second homotopy group, $\pi_2(\mathcal{O}_P) \cong \mathbb{Z}$ [32]. For the ferromagnetic spinor the order parameter space is $\mathcal{O}_F \cong \text{SO}(3)$ [28], and hence the second homotopy group is trivial, $\pi_2(\mathcal{O}_F) \cong 0$, forbidding the existence of topologically stable point defects [33]. As pointed out above, the Dirac monopoles we consider here are not point defects in the ferromagnetic order parameter but in the associated synthetic magnetic field, and may therefore exist at the termination points of vortex lines in the scalar degree of

freedom [18]. Dirac refers to such vortex lines as nodal lines in his original work [29] since the probability density of the associated wavefunction vanishes at the vortex core.

We create isolated monopole defects in the polar BEC by applying spin rotations to the spinor ζ using an external quadrupole magnetic field. The magnetic field is well approximated by

$$\mathbf{B}(\mathbf{r}', t) = b_q(x'\hat{\mathbf{x}}' + y'\hat{\mathbf{y}}' - z'\hat{\mathbf{z}}') + \mathbf{B}_{\text{bias}}(t), \quad (6)$$

where b_q is the quadrupole field strength, $\mathbf{B}_{\text{bias}}(t) = (B_{\text{bias},x}(t), B_{\text{bias},y}(t), B_{\text{bias},z}(t))^T$ is a uniform bias field and $\{\hat{\mathbf{x}}', \hat{\mathbf{y}}', \hat{\mathbf{z}}'\}$ are the Cartesian basis vectors. Here, we utilize a basis $(x', y', z') = (x, y, 2z)$. The monopole is created by slowly bringing the zero point of the magnetic field, $\mathbf{r}'_0(t) = (-B_{\text{bias},x}(t), -B_{\text{bias},y}(t), B_{\text{bias},z}(t))^T/b_q$, into the middle of the condensate [see Fig. 1(a-c)], such that $\hat{\mathbf{d}}$ follows the direction of the local magnetic field adiabatically.

The isolated monopole created in this way is a topological point defect defined by the nematic vector $\hat{\mathbf{d}}_m = (x'\hat{\mathbf{x}}' + y'\hat{\mathbf{y}}' - z'\hat{\mathbf{z}}')/r'$, where $r' = \sqrt{x'^2 + y'^2 + z'^2}$. It is related to the hedgehog monopole $\hat{\mathbf{d}}_h$, in which the nematic vector field points radially outwards from the location of the monopole, through a sign change and π rotation about the z axis, $\hat{\mathbf{d}}_h = -e^{-iF_z\pi}\hat{\mathbf{d}}_m = (x'\hat{\mathbf{x}}' + y'\hat{\mathbf{y}}' + z'\hat{\mathbf{z}}')/r'$. Thus, the two configurations, $\hat{\mathbf{d}}_m$ and $\hat{\mathbf{d}}_h$, both describe a point defect.

The spin configuration hosting a Dirac monopole can be defined by the spin vector $\mathbf{S}_D = |\mathbf{S}_D|(x'\hat{\mathbf{x}}' + y'\hat{\mathbf{y}}' - z'\hat{\mathbf{z}}')/r'$. Since point defects are not topologically allowed in the ferromagnetic phase of spin-1 BECs, this spin texture is naturally accompanied by one or more nodal lines connecting the boundary of the condensate with the core of the monopole. The nodal lines appear not in the condensate spin texture but in the atomic density. In previously realized Dirac monopoles [19], the nodal line is a doubly-quantized vortex connecting to the defect. This doubly-quantized vortex was observed to split into the more energetically favorable configuration containing two singly-quantized vortices [19, 34]. Indeed, in the ground-state Dirac monopole configuration [35], there are two single-quantum vortices connecting to the monopole. Furthermore, these nodal lines have vanishing particle density only in the pure ferromagnetic phase. For the Dirac monopoles obtained as a result of the decay of the isolated monopole, the nodal lines are expected to appear as two single-quantum vortices in the partially-depleted total particle density and as more distinct depletions in the spin density [30]. This indicates that the nodal lines are partly filled with polar atoms, and may therefore be referred to as polar-core vortices [35]. Recently, it was shown theoretically that in the absence of any external magnetic fields, the isolated monopole decays into a polar-core vortex with strictly nonvanishing particle density at the vortex core [36].

III. METHODS

A. Experimental methods

The experimental protocol employed in the creation of isolated monopoles is essentially identical to that in Ref. [20]. Our experiments begin with optically trapped ^{87}Rb atoms prepared in the polar internal state $\hat{\mathbf{z}} = (0, 1, 0)_Z^T$. A typical atom number is $N = 2.1 \times 10^5$ and the thermal cloud is observed to be negligibly small. The optical trapping frequencies are $\omega_r \approx 2\pi \times 130$ Hz and $\omega_z \approx 2\pi \times 170$ Hz. The strength of the gradient field is $b_q = 4.3$ G/cm and the field zero is moved into the condensate by linearly ramping a bias field, aligned with $\hat{\mathbf{z}}$, from 10 mG to zero in 40 ms. The vector field $\hat{\mathbf{d}}$ adiabatically follows the external magnetic field during the slow ramp, resulting in the isolated monopole configuration $\hat{\mathbf{d}}_m$.

Once the isolated monopole is created, we hold the zero point of the quadrupole field in the middle of the condensate for t_{hold} . We vary t_{hold} for different experimental runs, which provides us with information on the condensate dynamics at different stages of the decay. As the polar phase decays into the ferromagnetic phase, the magnetic order becomes defined by the local spin \mathbf{S} rather than $\hat{\mathbf{d}}$.

After holding the monopole in the presence of the quadrupole field for t_{hold} , we apply a projection ramp along a chosen quantization axis. This is implemented by rapidly increasing the bias field to a large value along the quantization axis such that $|\mathbf{B}_{\text{bias}}| \gg b_q R_p$, where R_p is the effective extent of the condensate. This ramp is sudden in the sense that the order parameter is expected to remain essentially unchanged, allowing us to project the order parameter to the eigenstates of the Zeeman Hamiltonian along the chosen quantization axis. The quadrupole contribution to the field is then quickly turned off and the condensate is released from the optical trap. During the subsequent 23.1-ms free expansion of the cloud, the bias field is adiabatically rotated into the x direction. A 3.5-ms pulse of current applied to the quadrupole field coils produces a magnetic gradient that separates the spin states horizontally. Finally, the bias field is rotated to point along the y axis and the condensate cloud with spatially separated spin states is simultaneously imaged along y and z . A detailed description of the projection ramp and the associated imaging methods are presented in Ref. [19].

B. Numerical methods

We numerically simulate our experiments by solving the dynamics of the mean-field order parameter Ψ according to the Gross-Pitaevskii (GP) equation and by employing the literature values for the constants. The

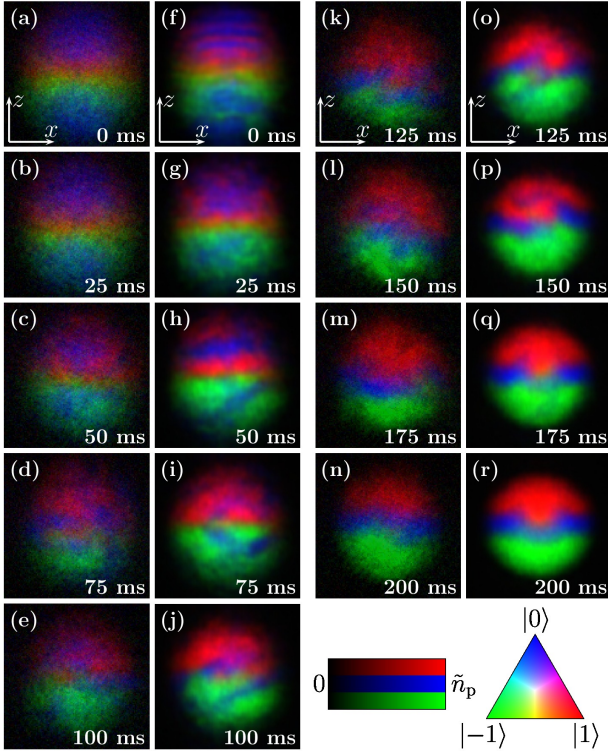


FIG. 2. Column particle densities imaged along y in the three $-z$ -quantized spin states during the decay of an isolated monopole for (a–e,k–n) experiments and (f–j,o–r) simulations. The hold times are indicated in the bottom right corner of each panel. The quadrupole field gradient is $b_q = 4.3$ G/cm. The peak particle density is $\tilde{n}_p = 8.5 \times 10^8$ cm $^{-2}$ and the field of view in each panel is 228×228 μm^2 .

GP equation reads

$$i\hbar \frac{\partial}{\partial t} \Psi(\mathbf{r}, t) = \{h(\mathbf{r}, t) + n(\mathbf{r}, t) [c_0 + c_2 \mathbf{S}(\mathbf{r}, t) \cdot \mathbf{F}] - i\Gamma n^2(\mathbf{r}, t)\} \Psi(\mathbf{r}, t), \quad (7)$$

where \hbar is the reduced Planck constant, $c_0 = 4\pi\hbar^2(a_0 + 2a_2)/(3m)$ and $c_2 = 4\pi\hbar^2(a_2 - a_0)/(3m)$ are the constants related to density–density and spin–spin interactions [24, 37], respectively, with the s -wave scattering lengths being $a_0 = 5.387$ nm and $a_2 = 5.313$ nm [38], and $m = 1.443 \times 10^{-25}$ kg being the mass of a ^{87}Rb atom. The three-body recombination rate is $\Gamma = \hbar \times 2.9 \times 10^{-30}$ cm 6 /s [39]. The single-particle Hamiltonian h is given by

$$h(\mathbf{r}, t) = -\frac{\hbar^2}{2m} \nabla^2 + V_{\text{opt}}(\mathbf{r}) + g_F \mu_B \mathbf{B}(\mathbf{r}, t) \cdot \mathbf{F}, \quad (8)$$

where V_{opt} is the optical trapping potential, $g_F = -1/2$ is the Landé g -factor, and μ_B is the Bohr magneton. The quadratic Zeeman shift is not included since it does not have a significant effect on the dynamics considered here [30]. The optical trap in the vicinity of the condensate is approximated by a harmonic potential $V_{\text{opt}} = m [\omega_r^2 (x^2 + y^2) + \omega_z^2 z^2] / 2$. The external mag-

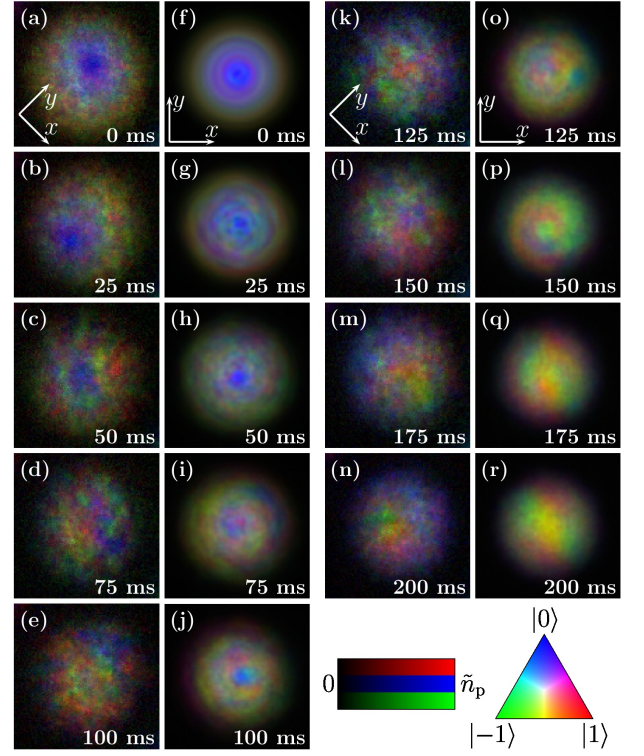


FIG. 3. As Fig. 2, but imaged along z with the peak particle density $\tilde{n}_p = 1.0 \times 10^9$ cm $^{-2}$.

netic field \mathbf{B} assumes the quadrupole configuration given by Eq. (6).

The ground state of the system is found by a relaxation method [40] with the bias field set along positive z such that $|\mathbf{B}_{\text{bias}}| \gg b_q Z$, where Z is the effective axial extent of the condensate along z . With the experimental parameters, the relaxation leads to an essentially spin-polarized ferromagnetic phase, $\zeta \approx (1, 0, 0)_Z^T$. Subsequently, the spinor components are swapped resulting in $\zeta \approx (0, 1, 0)_Z^T$. The experimental protocol is then simulated by solving the corresponding temporal evolution from Eq. (7). Here, we employ the split operator method together with fast Fourier transforms [40]. The computations are carried out on a discretized three-dimensional grid of size $200 \times 200 \times 200$ using graphics processing units.

IV. RESULTS

A. Decay of an isolated monopole

Figures 2 and 3 show the particle densities imaged along y and z , respectively, in different spin states during the decay of the isolated monopole. Hereafter, the images along y and z will be referred to as side and top images, respectively. Although the agreement between the experiments and the simulations is good in general, the loss of atoms from the trap due to the anharmonicity

of the optical potential is not included in the simulations, resulting in a slight disagreement in the contrast of the images. At $t_{\text{hold}} = 0$ ms, the $-z$ -quantized spinor component ζ_0 occupies the top and the bottom parts of the condensate cloud, while the spinor components $\zeta_{\pm 1}$ occupy the middle region with partial overlap as observed in the side images. As is evident from Eq. (4), the structure is consistent with the polar spinor with the vector field $\hat{\mathbf{d}}$ oriented along the local quadrupole magnetic field. The $\zeta_{\pm 1}$ components do not fully overlap due to the fact that the projection ramp is applied before the quadrupole field is completely switched off. In the top images, the $\zeta_{\pm 1}$ components form a ring around the ζ_0 component. These are the characteristic indications that an isolated monopole has been created in the condensate cloud [20].

At $t_{\text{hold}} = 25$ ms, the monopole structure is still visible, with ζ_{+1} and ζ_{-1} spinor components being displaced slightly to the top and bottom parts of the condensate, respectively. At $t_{\text{hold}} = 50$ ms, the $\zeta_{\pm 1}$ components have continued to displace, and in addition, the ζ_0 component has moved towards the center region. At $t_{\text{hold}} = 100$ ms, this movement has continued further and the density depletion initially visible in the top images in the $\zeta_{\pm 1}$ components is no longer distinguishable. Here, the condensate is far from the pure polar phase, and consequently the isolated monopole structure is not well-defined.

For $125 \text{ ms} \leq t_{\text{hold}} \leq 150$ ms, the condensate is nearly in the pure ferromagnetic phase, as indicated by the well-separated spin states in the side images. Finally, at $t_{\text{hold}} = 200$ ms, the spin configuration in the side image accurately corresponds to the Dirac monopole illustrated in Fig. 1(d) [19]. At this time, the spinor components ζ_{+1} , ζ_0 , and ζ_{-1} occupy the top, middle, and bottom parts of the condensate, respectively. In the top images, after $t_{\text{hold}} = 100$ ms, all three spin states overlap as expected for the Dirac monopole. Thus, in both the simulations and the experiments, the condensate has continuously decayed from the isolated monopole to the spin configuration of a Dirac monopole.

B. Observation of nodal lines

The column particle densities of condensates showing the nodal lines associated with the Dirac monopole are presented in Fig. 4. As noted above, Dirac's theory requires the existence of nodal lines, as does the topological constraint forbidding the existence of a point defect in the ferromagnetic phase. A pair of singly-quantized vortex lines appears spontaneously during the decay, connecting the core of the monopole to the condensate boundary. The nodal lines are not observed as a doubly-quantized vortex, as they were in the experiments detailed in Ref. [19], because the configuration with two singly-quantized vortices is energetically more favorable. Furthermore, it is energetically favorable for the nodal lines to minimize their length [35] such that they tend to terminate at the condensate boundary that is closest to

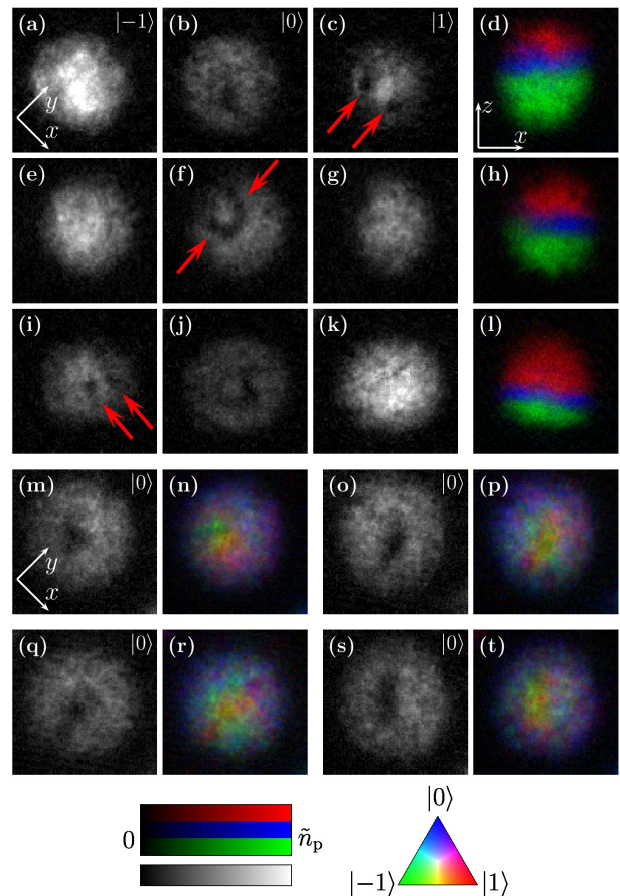


FIG. 4. Experimental column particle densities of $-z$ -quantized spin states showing nodal lines associated with the Dirac monopole. In (a-l), the first, second, and third columns correspond to the top images of ζ_{-1} , ζ_0 , and ζ_{+1} spinor components, respectively, and the fourth column shows the corresponding composite side image. In (a-d), the monopole is located in the top part of the condensate, in (e-h) in the middle, and in (i-l) in the bottom part. The red arrows indicate the locations of the nodal lines. In (m-t), each set of two adjacent images is extracted from an individual experiment in which the monopole is located in the middle of the condensate, such that (m,o,q,s) show the column particle density of ζ_0 spinor component and (n,p,r,t) show the corresponding composite top image, respectively. The data for (m,n) are the same as in Fig. 3(n). The hold time for (a-d) is 400 ms, for (e-h) 225 ms, for (i-l) 400 ms, for (m,n) 200 ms, for (o,p) 150 ms, for (q,r) 175 ms, and for (s,t) 200 ms. The field of views are as in Fig. 2, and the peak particle densities are (a-c,e-g,i-k,m,o,q,s) $\tilde{n}_p = 5.0 \times 10^8 \text{ cm}^{-2}$, (d,h,l) $\tilde{n}_p = 8.5 \times 10^8 \text{ cm}^{-2}$, and (n,p,r,t) $\tilde{n}_p = 1.0 \times 10^9 \text{ cm}^{-2}$.

the monopole. Although not shown, simulations reveal that the vortex associated with the nodal line changes its vorticity at the core of the monopole. The nodal lines are observed in roughly 90% of the one hundred different experiments conducted for $t_{\text{hold}} \geq 150$ ms. We attribute the absence of observed nodal lines in some experimental realizations to occasional magnetic field excursions that displace the monopole to positions very close to the con-

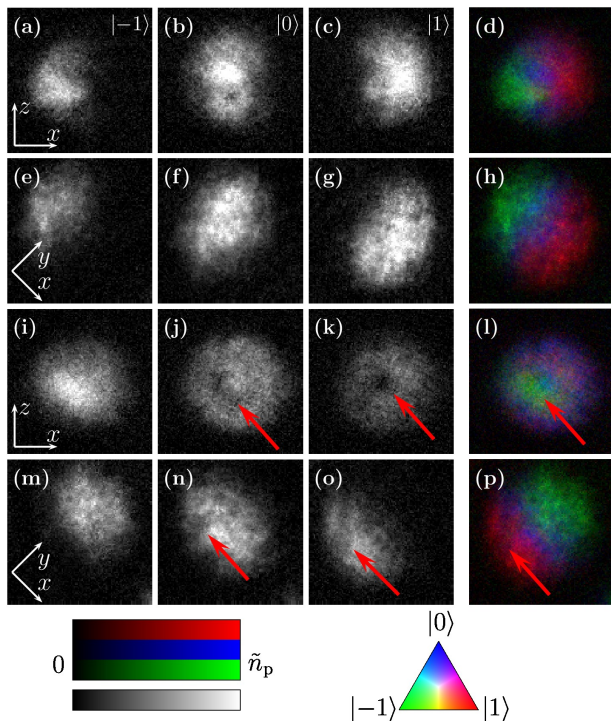


FIG. 5. Experimental column particle densities of (a-h) x - and (i-p) $-y$ -quantized spin states. First, second, and third columns correspond to spinor components ζ_{-1} , ζ_0 , and ζ_{+1} , respectively, and the fourth column shows the corresponding composite image. The red arrows indicate the locations of the nodal lines. The field of views are as in Fig. 2, and the peak particle densities are (a-c,e-g,i-k,m-o) $\tilde{n}_p = 5.0 \times 10^8 \text{ cm}^{-2}$, (d,l) $\tilde{n}_p = 8.5 \times 10^8 \text{ cm}^{-2}$, and (h,p) $\tilde{n}_p = 1.0 \times 10^9 \text{ cm}^{-2}$.

densate boundary.

As shown in Fig. 4(a-d), if the monopole is located in the top part of the condensate, the nodal line is typically observed as two density-depleted holes in the $-z$ -quantized ζ_{+1} spinor component. Contrariwise, if the monopole is located in the bottom part of the condensate, as shown in Fig. 4(i-l), the nodal line extends to the bottom of the condensate and is observed in the density depletions in the ζ_{-1} component. If the monopole is created in the middle of the condensate, the nodal lines are typically oriented in the xy plane, and they are observed as density-depleted lines in the ζ_0 component, as shown in Fig. 4(e-h,m-t). In some experimental realizations, the horizontal nodal lines partially extend into the ζ_{+1} or ζ_{-1} components. These observations are in agreement with theoretical expectations [30, 35] for nodal lines associated with the Dirac monopole.

Additional vortices can sometimes appear in the condensate during the BEC creation process or due to the presence of oscillating magnetic fields during the decay (see Appendix). These accidental vortices align themselves with the z axis to minimize their length. Whereas the accidental vortices pierce the length of the entire condensate along its short direction, parallel to the z axis,

the nodal lines we observe extend from the monopole core to the nearest boundary. Our ability to control the location of the nodal lines by positioning the magnetic field zero is an indication that the nodal lines are not produced by accidental vortices.

C. Characterization of the spin configuration of a Dirac monopole

The particle densities of the x - and $-y$ -quantized spin states for $t_{\text{hold}} = 200 \text{ ms}$ are shown in Fig. 5. We observe that the spin configuration corresponds to that of the Dirac monopole independent of the chosen quantization axis. These observations extend those of Ref. [19], in which the spin configuration associated with the Dirac monopole was only characterized with the quantization axis parallel to z . Furthermore, for the specific $-y$ projection shown in Fig. 5(i-p), the nodal line extends from the origin toward the $-y$ axis and manifests itself as a density depletion in the ζ_0 and ζ_{+1} spinor components.

D. Rate of the monopole decay

We investigate the time scales related to the decay process by calculating the magnetization parameter along z , M_z , for different hold times t_{hold} . We define the magnetization parameter as

$$M_z = \frac{1}{N} \int dz \int dx |n_{+1}^y(x, z) - n_{-1}^y(x, z)|, \quad (9)$$

where $n_{m_z}^y = \int dy n |\zeta_{m_z}|^2$ is the y -integrated particle density in the spin state corresponding to the magnetic quantum number m_z . The $-z$ -quantized $\zeta_{\pm 1}$ spinor components move in opposite vertical directions due to the nonzero gradient present during the projection ramp. Here, we apply a compensating shift in the vertical direction such that for $t_{\text{hold}} = 0 \text{ ms}$ the $\zeta_{\pm 1}$ components overlap, yielding a minimum value for M_z . An identical correction is applied to all the data. As the condensate decays into the ferromagnetic phase, the magnetization parameter increases.

Figure 6 shows the magnetization parameter of the BEC as a function of the hold time in the presence of two different gradient field strengths, 2.2 G/cm and 4.3 G/cm. In both cases the isolated monopole is created with $b_q = 4.3 \text{ G/cm}$, after which b_q is linearly ramped to its chosen value during the first 10 ms of the evolution. During the ramping of b_q , we adjust the bias fields accordingly to keep the field zero approximately centered in the middle of the condensate cloud. With the weaker gradient, M_z reaches its asymptotic value of approximately 0.35 at $t_{\text{hold}} \approx 80 \text{ ms}$ with an approximate rate 2.4 1/s. For $t_{\text{hold}} \geq 100 \text{ ms}$ we can identify the Dirac monopole spin configuration and the nodal lines from the experimental particle densities (data not shown). With the

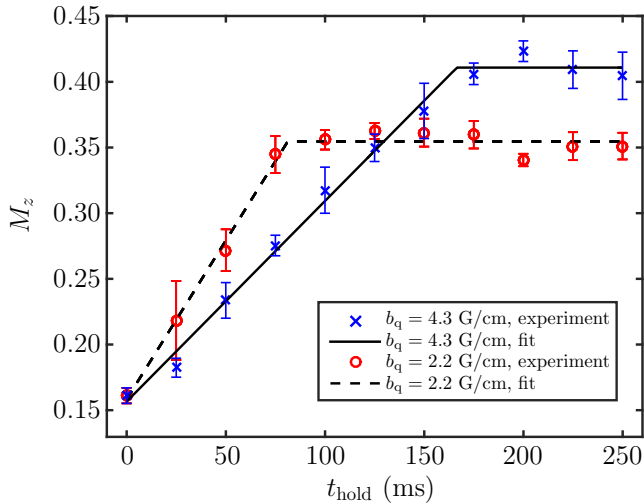


FIG. 6. Magnetization parameter M_z as a function of hold time t_{hold} . Blue crosses and red circles represent the mean value of ten individual experiments with magnetic field gradients $b_q = 4.3$ G/cm and $b_q = 2.2$ G/cm, respectively. The error bars indicate the uncertainty of two standard deviations of the means. Solid and dashed lines are piecewise linear fitting functions with constant ends.

stronger gradient, the asymptotic value of approximately 0.41 is reached at $t_{\text{hold}} \approx 170$ ms with an approximate rate 1.5 1/s. Assuming an ideal quadrupole spin configuration, as well as a Thomas–Fermi distribution with the ratio of the radii being $Z/R \approx 1.2$, we obtain an estimate for the theoretical maximum value $M_z \approx 0.55$. The saturation values of M_z should be compared to this maximum value.

The decay process is slower in the presence of a stronger field gradient since there is less spatial overlap between the emerging spin domains [30]. Differences in the degree of spatial overlap of the spin domains is also the reason for differences in the asymptotic values of the magnetization for different magnetic field gradients.

V. CONCLUSION

We have experimentally studied the decay dynamics of isolated monopoles in spin-1 BECs of ^{87}Rb atoms. While the condensate experiences a dynamical quantum phase transition from the polar to the ferromagnetic phase, the isolated monopole decays into a spin configuration with a Dirac monopole in its synthetic magnetic field. These results are obtained by analyzing the experimental column particle densities of all spin states projected along different axes. We have also identified the nodal lines associated with the emergent Dirac monopole. Numerical simulations are in agreement with these experimental results without free parameters. The decay of the monopole is faster in weaker magnetic fields. We at-

tribute this behavior to the polar phase being less stable in weaker magnetic fields.

To date, experimental studies of spatially-localized monopoles in spinor BECs have been limited to two publications [19, 20] (see also Ref. [41]). Our work further verifies the existence of both isolated and Dirac monopoles through reproduction and in-depth characterization. For future experiments, even more precise control of the experimental parameters is desirable in order to probe the delicate structure of different types of topological defects appearing in spinor BECs. Future studies on the stability and the dynamics of, e.g., knot solitons [22], could be first steps in this direction. Furthermore, the experimental realization of the vortex pump in spinor BECs remains a future challenge requiring precise control of the experimental parameters that determine the dynamics of the atomic cloud [42].

ACKNOWLEDGMENTS

We acknowledge funding by the National Science Foundation (grant PHY-1519174), by the Academy of Finland through its Centres of Excellence Program (grant No. 251748 and No. 284621), by the European Research Council under Consolidator Grant No. 681311 (QUESS), the Magnus Ehrnrooth Foundation, and the Education Network in Condensed Matter and Materials Physics. CSC–IT Center for Science Ltd. (Project No. ay2090) and Aalto Science-IT project are acknowledged for computational resources.

Appendix: Emergence of vortices due to moving magnetic field zero point

The addition of an oscillating magnetic field at the 60-Hz line frequency causes the location of the zero point of the magnetic field to oscillate about its central position. It introduces many additional singly-quantized vortices in the condensate during the decay of the isolated monopole, as shown in Fig. 7. Qualitatively similar results with approximately 15 vortices are obtained in the simulations under conditions in which the magnetic field zero rotates about the center of the condensate in the xy plane. Note that the comparison between theory and experiment in Fig. 7 is qualitative because the experimental trajectory of the field zero was not characterized in detail. In contrast to the nodal line studied in Fig. 4, which is typically bent and not aligned with the z axis, the additional vortices observed here are consistently aligned with the z axis for a well-centered Dirac monopole and tend to appear in all three spin components. Similar emergence of vortices has previously been observed with the driving of the zero point of the external magnetic field outside the condensate, giving rise to an effective Lorentz force [43].

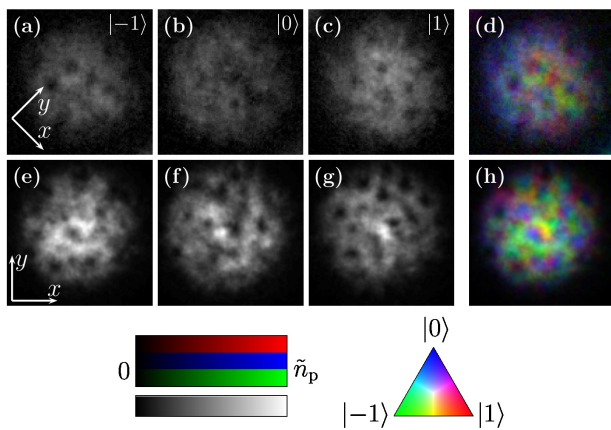


FIG. 7. (a–d) Experimental column particle densities of $-z$ -quantized spin states and (e–h) numerical column particle densities with a circularly rotating field zero in the xy plane corresponding to the magnetic field peak-to-peak amplitude of 1 mG and 60-Hz oscillation frequency. Here, the hold time is $t_{\text{hold}} = 100$ ms. First, second, and third columns correspond to the spinor components ζ_{-1} , ζ_0 , and ζ_{+1} , respectively, and the fourth column shows the corresponding composite image. The field of view and the peak particle densities are identical to those in Fig. 3.

-
- [1] M. H. Anderson, J. R. Ensher, M. R. Matthews, C. E. Wieman, and E. A. Cornell, “Observation of Bose-Einstein condensation in a dilute atomic vapor,” *Science* **269**, 198 (1995).
 - [2] K. B. Davis, M. O. Mewes, M. R. Andrews, N. J. van Druten, D. S. Durfee, D. M. Kurn, and W. Ketterle, “Bose-Einstein condensation in a gas of sodium atoms,” *Phys. Rev. Lett.* **75**, 3969 (1995).
 - [3] M. Ueda, “Topological aspects in spinor Bose-Einstein condensates,” *Rep. Prog. Phys.* **77**, 122401 (2014).
 - [4] M. R. Matthews, B. P. Anderson, P. C. Haljan, D. S. Hall, C. E. Wieman, and E. A. Cornell, “Vortices in a Bose-Einstein condensate,” *Phys. Rev. Lett.* **83**, 2498 (1999).
 - [5] A. E. Leanhardt, A. Görlitz, A. P. Chikkatur, D. Kielpinski, Y. Shin, D. E. Pritchard, and W. Ketterle, “Imprinting vortices in a Bose-Einstein condensate using topological phases,” *Phys. Rev. Lett.* **89**, 190403 (2002).
 - [6] A. L. Fetter, “Rotating trapped Bose-Einstein condensates,” *Rev. Mod. Phys.* **81**, 647 (2009).
 - [7] G. D. Telles, P. E. S. Tavares, A. R. Fritsch, A. Cidrim, V. S. Bagnato, A. C. White, A. J. Allen, and C. F. Barenghi, “Twisted unwinding of multi-charged quantum vortex and generation of turbulence in atomic Bose-Einstein condensates,” arXiv:1505.00616.
 - [8] T. Mizushima, K. Machida, and T. Kita, “Mermin-Ho vortex in ferromagnetic spinor Bose-Einstein condensates,” *Phys. Rev. Lett.* **89**, 030401 (2002).
 - [9] A. E. Leanhardt, Y. Shin, D. Kielpinski, D. E. Pritchard, and W. Ketterle, “Coreless vortex formation in a spinor Bose-Einstein condensate,” *Phys. Rev. Lett.* **90**, 140403 (2003).
 - [10] S. W. Seo, S. Kang, W. J. Kwon, and Y.-i. Shin, “Half-quantum vortices in an antiferromagnetic spinor Bose-Einstein condensate,” *Phys. Rev. Lett.* **115**, 015301 (2015).
 - [11] S. Donadello, S. Serafini, M. Tylutki, L. P. Pitaevskii, F. Dalfovo, G. Lamporesi, and G. Ferrari, “Observation of solitonic vortices in Bose-Einstein condensates,” *Phys. Rev. Lett.* **113**, 065302 (2014).
 - [12] U. Al Khawaja and H. Stoof, “Skyrmions in a ferromagnetic Bose-Einstein condensate,” *Nature (London)* **411**, 918 (2001).
 - [13] L. S. Leslie, A. Hansen, K. C. Wright, B. M. Deutsch, and N. P. Bigelow, “Creation and detection of skyrmions in a Bose-Einstein condensate,” *Phys. Rev. Lett.* **103**, 250401 (2009).
 - [14] J.-Y. Choi, W. J. Kwon, and Y.-I. Shin, “Observation of topologically stable 2D skyrmions in an antiferromagnetic spinor Bose-Einstein condensate,” *Phys. Rev. Lett.* **108**, 035301 (2012).
 - [15] H. T. C. Stoof, E. Vliegen, and U. Al Khawaja, “Monopoles in an antiferromagnetic Bose-Einstein condensate,” *Phys. Rev. Lett.* **87**, 120407 (2001).
 - [16] C. M. Savage and J. Ruostekoski, “Dirac monopoles and dipoles in ferromagnetic spinor Bose-Einstein condensates,” *Phys. Rev. A* **68**, 043604 (2003).
 - [17] V. Pietilä and M. Möttönen, “Non-Abelian magnetic monopole in a Bose-Einstein condensate,” *Phys. Rev. Lett.* **102**, 080403 (2009).
 - [18] V. Pietilä and M. Möttönen, “Creation of Dirac monopoles in spinor Bose-Einstein condensates,” *Phys. Rev. Lett.* **103**, 030401 (2009).

- [19] M. W. Ray, E. Ruokokoski, S. Kandel, M. Möttönen, and D. S. Hall, “*Observation of Dirac monopoles in a synthetic magnetic field*,” *Nature (London)* **505**, 657 (2014).
- [20] M. W. Ray, E. Ruokokoski, K. Tiurev, M. Möttönen, and D. S. Hall, “*Observation of isolated monopoles in a quantum field*,” *Science* **348**, 544 (2015).
- [21] Y. Kawaguchi, M. Nitta, and M. Ueda, “*Knots in a spinor Bose-Einstein condensate*,” *Phys. Rev. Lett.* **100**, 180403 (2008).
- [22] D. S. Hall, M. W. Ray, K. Tiurev, E. Ruokokoski, A. H. Gheorghe, and M. Möttönen, “*Tying quantum knots*,” *Nat. Phys.* **12**, 478 (2016).
- [23] J. Ruostekoski and J. R. Anglin, “*Monopole core instability and Alice rings in spinor Bose-Einstein condensates*,” *Phys. Rev. Lett.* **91**, 190402 (2003).
- [24] T.-L. Ho, “*Spinor Bose condensates in optical traps*,” *Phys. Rev. Lett.* **81**, 742 (1998).
- [25] M. Ueda and M. Koashi, “*Theory of spin-2 Bose-Einstein condensates: Spin correlations, magnetic response, and excitation spectra*,” *Phys. Rev. A* **65**, 063602 (2002).
- [26] Y.-J. Lin, R. L. Compton, K. Jimenez-Garcia, J. V. Porto, and I. B. Spielman, “*Synthetic magnetic fields for ultracold neutral atoms*,” *Nature (London)* **462**, 628 (2009).
- [27] J. Dalibard, F. Gerbier, G. Juzeliūnas, and P. Öhberg, “*Colloquium: Artificial gauge potentials for neutral atoms*,” *Rev. Mod. Phys.* **83**, 1523 (2011).
- [28] Y. Kawaguchi and M. Ueda, “*Spinor Bose-Einstein condensates*,” *Phys. Rep.* **520**, 253 (2012).
- [29] P. A. M. Dirac, “*Quantised singularities in the electromagnetic field*,” *Proc. R. Soc. Lond. A* **133**, 60 (1931).
- [30] K. Tiurev, E. Ruokokoski, H. Mäkelä, D. S. Hall, and M. Möttönen, “*Decay of an isolated monopole into a Dirac monopole configuration*,” *Phys. Rev. A* **93**, 033638 (2016).
- [31] F. Zhou, “*Spin correlation and discrete symmetry in spinor Bose-Einstein condensates*,” *Phys. Rev. Lett.* **87**, 080401 (2001).
- [32] M. Nakahara, *Geometry, Topology and Physics*, 2nd ed. (Taylor & Francis Group, Boca Raton, FL, 2003).
- [33] H. Mäkelä, Y. Zhang, and K.-A. Suominen, “*Topological defects in spinor condensates*,” *J. Phys. A: Math. and Gen.* **36**, 8555 (2003).
- [34] M. Möttönen, T. Mizushima, T. Isoshima, M. M. Salomaa, and K. Machida, “*Splitting of a doubly quantized vortex through intertwining in Bose-Einstein condensates*,” *Phys. Rev. A* **68**, 023611 (2003).
- [35] E. Ruokokoski, V. Pietilä, and M. Möttönen, “*Ground-state Dirac monopole*,” *Phys. Rev. A* **84**, 063627 (2011).
- [36] K. Tiurev, P. Kuopanportti, A. M. Gunyhó, M. Ueda, and M. Möttönen, “*Evolution of an isolated monopole in a spin-1 Bose-Einstein condensate*,” *Phys. Rev. A* **94**, 053616 (2016).
- [37] T. Ohmi and K. Machida, “*Bose-Einstein condensation with internal degrees of freedom in alkali atom gases*,” *J. Phys. Soc. Jpn.* **67**, 1822 (1998).
- [38] E. G. M. van Kempen, S. J. J. M. F. Kokkermans, D. J. Heinzen, and B. J. Verhaar, “*Interisotope determination of ultracold rubidium interactions from three high-precision experiments*,” *Phys. Rev. Lett.* **88**, 093201 (2002).
- [39] E. A. Burt, R. W. Ghrist, C. J. Myatt, M. J. Holland, E. A. Cornell, and C. E. Wieman, “*Coherence, correlations, and collisions: What one learns about Bose-Einstein condensates from their decay*,” *Phys. Rev. Lett.* **79**, 337 (1997).
- [40] W. H. Press, S. A. Teukolsky, W. T. Vetterling, and B. P. Flannery, *Numerical Recipes in FORTRAN: The Art of Scientific Computing* (Cambridge University Press, Cambridge, 1994).
- [41] S. Sugawa, F. Salces-Carcoba, A. R. Perry, Y. Yue, and I. B. Spielman, “*Observation of a non-Abelian Yang monopole: From new Chern numbers to a topological transition*,” *arXiv:1610.06228*.
- [42] M. Möttönen, V. Pietilä, and S. M. M. Virtanen, “*Vortex pump for dilute Bose-Einstein condensates*,” *Phys. Rev. Lett.* **99**, 250406 (2007).
- [43] J.-Y. Choi, S. Kang, S. W. Seo, W. J. Kwon, and Y.-I. Shin, “*Observation of a geometric Hall effect in a spinor Bose-Einstein condensate with a skyrmion spin texture*,” *Phys. Rev. Lett.* **111**, 245301 (2013).